Electronic Supplementary Material (ESI) for ChemComm.
This journal is © The Royal Society of Chemistry 2020

Supporting Information for:

A Facile Carbon Fiber-sewed High Areal Density Electrode for Lithium Sulfur Batteries

*Mengxue He, ‡[a] Yaqi Li, ‡[a] Songsong Liu, [a] Rui Guo,[b] Yulin Ma,[a] Jingying Xie,[b] Hua Huo, [a] Xinqun Cheng,[a] Geping Yin,[a] Pengjian Zuo,[a]**

[a.] MIIT Key Laboratory of Critical Materials Technology for New Energy Conversion and Storage, School of Chemical Engineering and Technology, Harbin Institute of Technology, Harbin 150001, China

[b.] State Key Laboratory of Space Power Technology, Shanghai Institute of Space Power-sources, Shanghai 200245, China

** Corresponding author: zuopj@hit.edu.cn;*

Tel: 86-451-86403961; Fax: 86-451-86403961

‡These authors contributed equally to this work.

1. Experimental

2.1 Preparation of carbon/sulfur composite

Carbon/sulfur composites were prepared with melting diffusion method in a sealed Teflon container by heating pre-mixed sulfur and carbon at a weight ratio of 3:2 for 12 h under 155 °C. The KB (Ketjen Black, ECP600 JD) and CNT (L-MWNT-60100) were chosen as the sulfur host and the active materials are denoted as KB/S-60% and CNT/S-60%. In addition, KB/S-50 wt% was prepared by the same method with a weight ratio of 1:1.

2.2 Preparation of thick electrode and its Characterization

The slurry without carbon fiber was prepare by mixing the carbon/sulfur composite, acetylene black conductive carbon and binder with a mass ratio of 8:1:1 in deionized water. The slurry of the carbon fiber linked electrode was prepare by mixing the carbon/sulfur composite, acetylene black conductive carbon, binder and carbon fiber (M40JB-6000) with a mass ratio of 80:5:5:10 in deionized water. Carbon fiber was dipped in acetone at 50 ℃ over night before used. Electrode was prepared by coating the slurry onto carbon-coated aluminum current collector via doctor-blade coating method, following drying in a vacuum oven at 50 ℃ overnight. It was punched into small circular disks (10 mm in diameter).

2.3 Physical characterization

The morphology and microstructure of the prepared composites and the CF-sewed electrode were characterized by scanning electronic microscopy (FESEM, Hitachi S-4800). The X-ray diffraction measurements of the samples were performed using an X-ray powder diffractometer with Cu-Ka radiation source. The content of sulfur in the composites was confirmed using thermogravimetric analysis (TGA) via a simultaneous thermal analysis (DSC, Netzsch STA449F3) in argon at 10 ℃ min^{-1}. The specific surface area and pore size distribution of the samples were determined by N2 adsorption-desorption isotherms using a 3H-2000PS1 gas adsorption analyzer.

2.4 Electrochemical Tests

The electrochemical performance of the high sulfur loading electrode was evaluated by CR2032 coin cell using the metallic lithium as counter electrode and Celgard 2400 membrane as separator. The electrolyte contained 1 mol L^{-1} lithium bis(trifluoromethane sulfonyl) imide (LiTFSI, 99.9%, aladdin) in a binary solvent of 1,3-dioxolane (DOL, aladdin) and dimethoxyethane (DME, aladdin) (1:1 in volume) with 0.4 M lithium nitrate ($LiNO_3$, aladdin) as additive. The amount of electrolyte used in this work was E/S=12 μL mg^{-1}. All the operations were carried out in an Ar-filled glove box. Galvanostatic charge-discharge cycling test was carried out at room temperature using NEWARE battery cycler (China) between 1.6 and 2.8 V. Cyclic voltammetry (CV) study of the electrode

was recorded on an electrochemical work station between 1.2 and 3.0 V at a scan rate of 0.025 mV s^{-1}. All potentials presented in this study were quoted versus the Li/Li^+ scale. The LiF-modified Li anode was prepared by the vacuum evaporation process. In the vacuum environment, lithium fluoride powders were vaporized by heating, then the lithium fluoride steam was attached to the lithium surface, forming a lithium fluoride layer.

2. Figures:

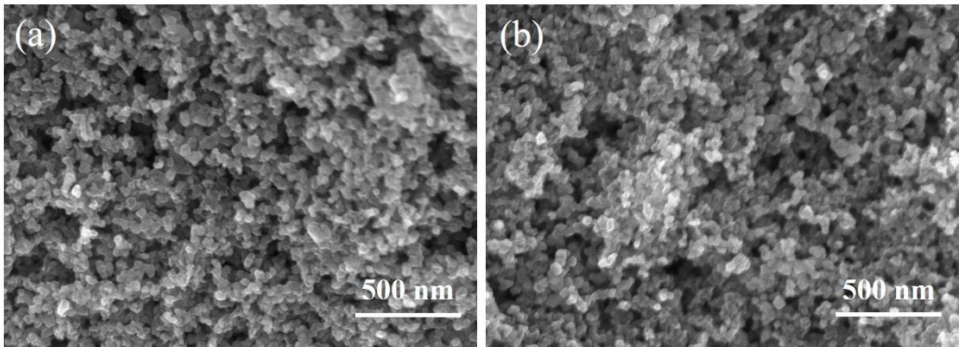

Fig. S1 SEM images of the (a) KB and (b) KB/S-60% composites.

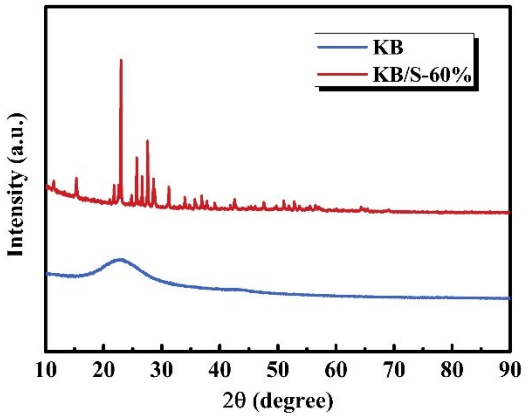

Fig. S2 XRD pattens of the KB and KB/S-60% composites.

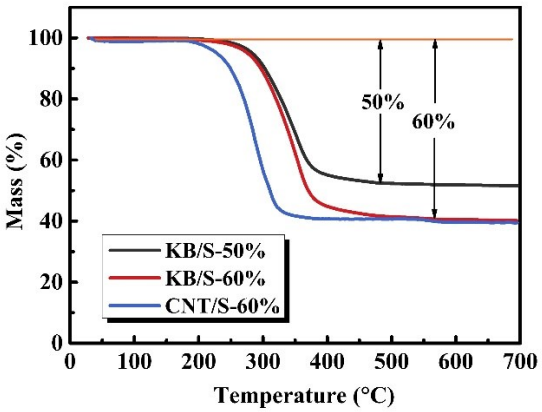

Fig. S3 TGA curves of the carbon/sulfur composites.

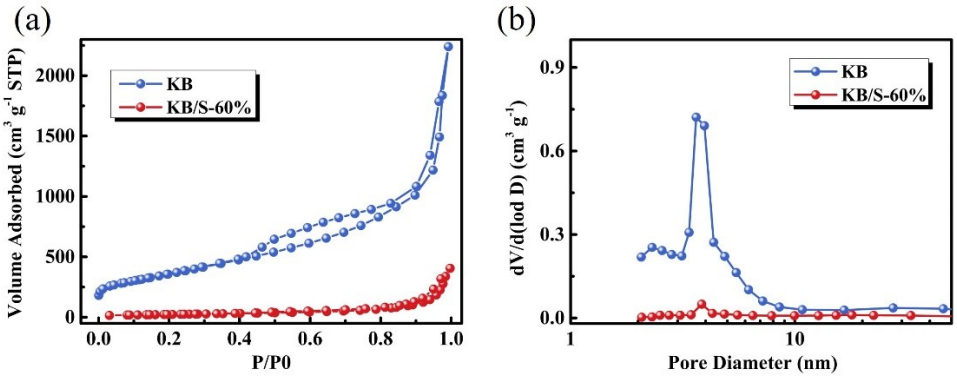

Fig. S4 (a) N_2 adsorption-desorption isotherms and (b) corresponding pore size distributions of the KB and KB/S-60%.

The SEM image demonstrates that the diameter of KB particles is between 60 and 80 nm, and it shows little change after compositing with sulfur (Fig. S1). Fig. S2 shows the e X-ray diffraction (XRD) patterns of the KB and KB/S-60% composites. There exist two broad peaks at around 23° and 43° in XRD pattern of KB, indicating the amorphous state of carbon. Diffraction peaks at 23° and 28° in XRD pattern of KB/S-60% correspond to the Fddd orthorhombic phase of sulfur (PDF # 08-0247). Thermal gravimetric analysis (TGA) was conducted to determine the sulfur contents

in the carbon/sulfur composites (Fig. S3). These samples display continuous weight loss from 200 to 400 ℃ in argon environment. The weight loss is 60% in the KB/S-60% and CNT/S-60%, and KB/S-50% demonstrates a weight loss of 50%. Brunauer-Emmett-Teller (BET) analysis of the N_2 adsorption isotherms of KB indicates a high surface area of 1300 m^2 g^{-1} and high pore volumes of 2.8 cm^3 g^{-1}, respectively (Fig. S4). After sulfur-impregnation of KB, the KB/S-60% shows the markedly decreased surface areas of 86 m^2 g^{-1} and pore volumes of 0.5 cm^3 g^{-1}, indicating intensive impregnation of sulfur into the pores of KB.

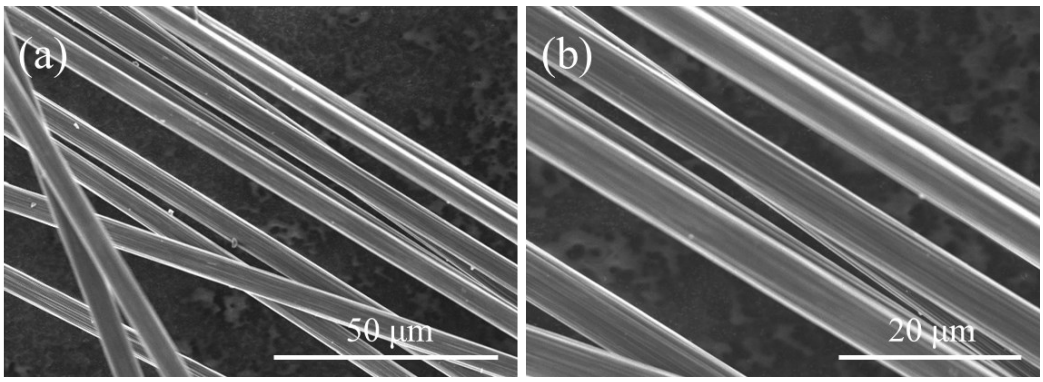

Fig. S5 SEM images of the carbon fibers in different resolution.

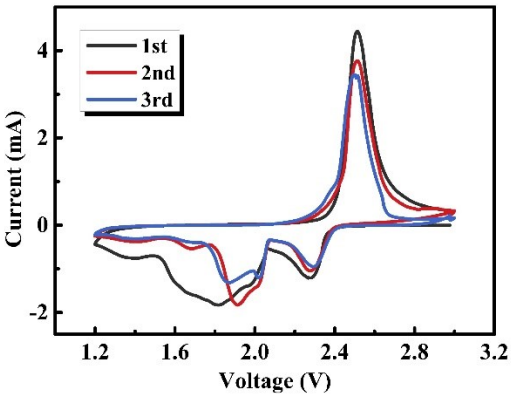

Fig. S6 CV curves of the thick electrode with KB/S-60% at 0.02 mV s^{-1}.

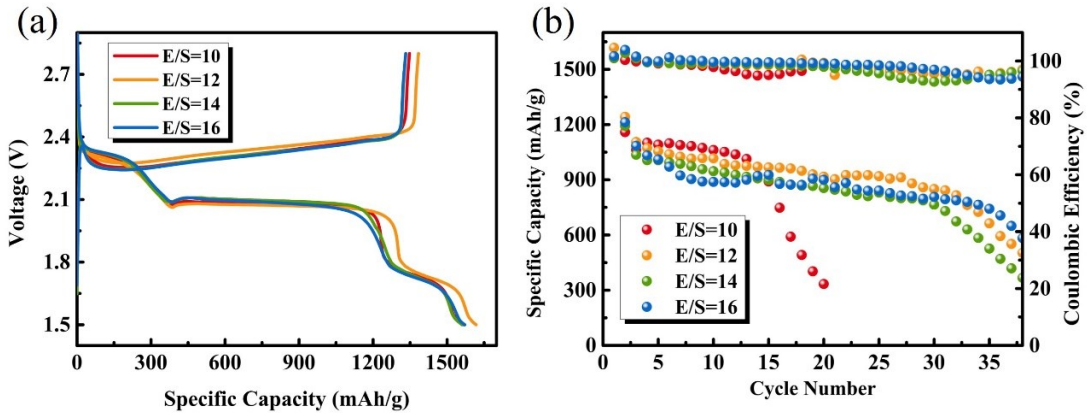

Fig. S7 (a) Discharge/charge curves at 0.05 C and (b) cycling performance at 0.1 C of the cell with different E/S μL mg^{-1}.

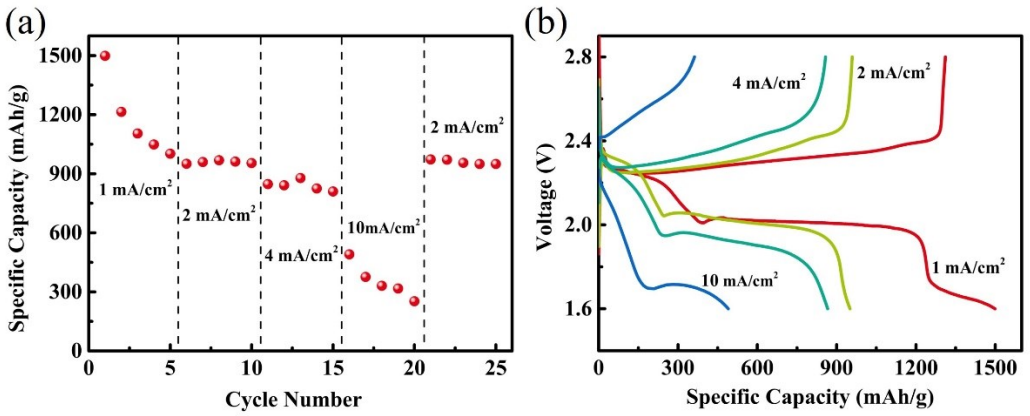

Fig. S8 (a) Rate performance and (b) the corresponding discharge/charge curves of the CF-sewed electrode at different current density (1 mA cm^{-2} equals to 0.05 C).

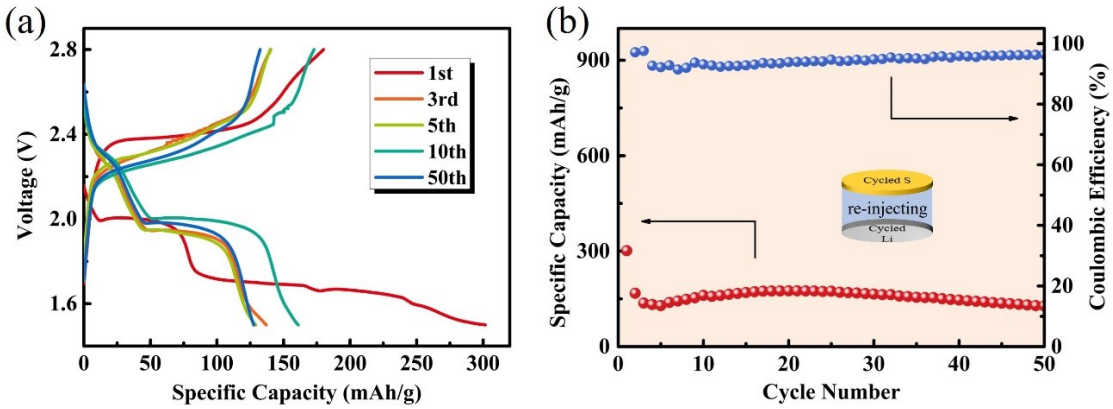

Fig. S9 (a) The discharge/charge curves and (b) cycling performance at 0.1 C of the cycled cell with re-inject electrolyte of 80 μL.

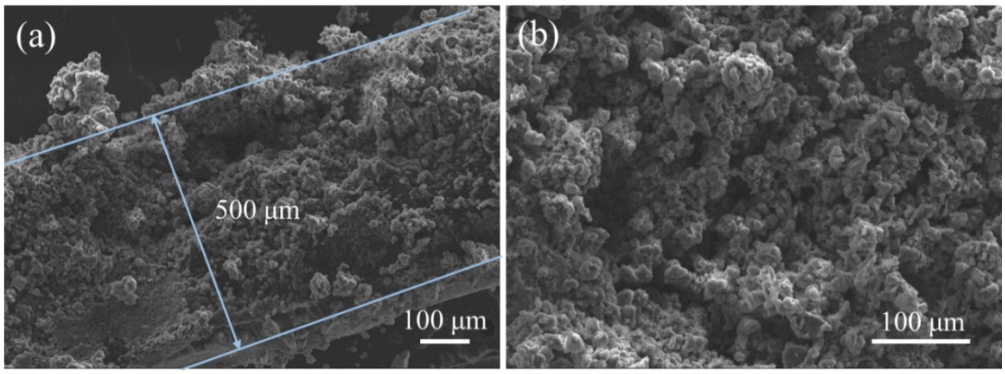

Fig. S10 SEM images of lithium anode after 40 cycles: (a) at cross section and (b) at surface.

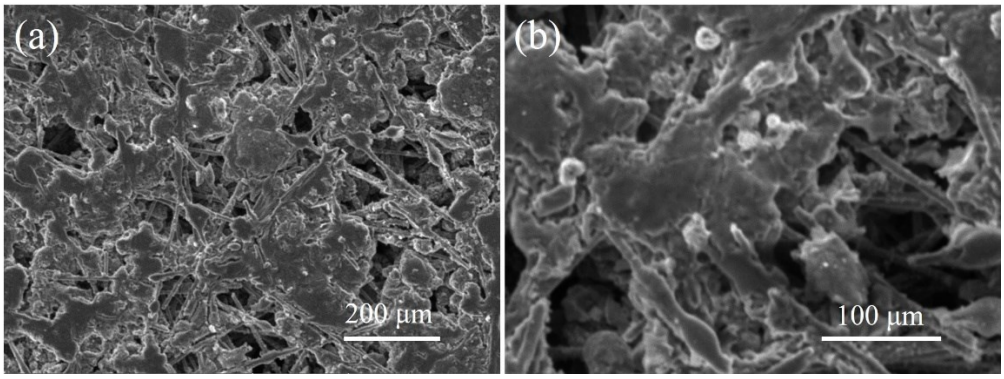

Fig. S11 SEM images of cycled CF-sewed electrolyte.

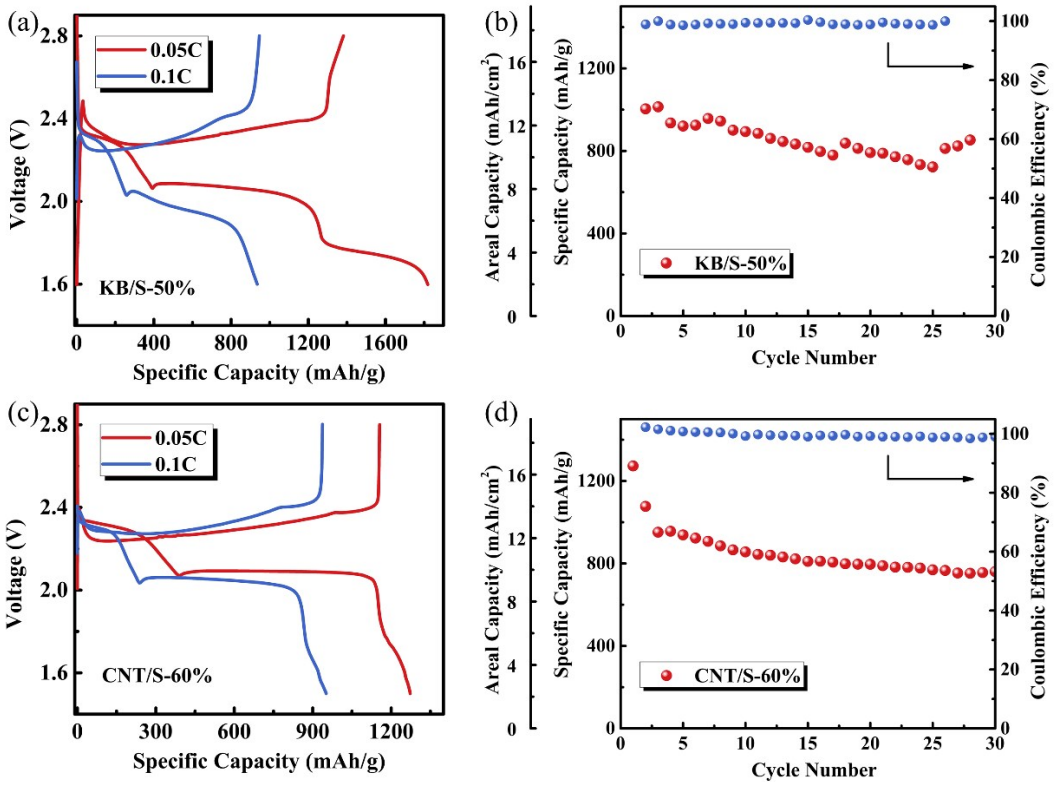

Fig. S12 (a) Discharge/charge curves and (b) cycling performance of KB/S-50% electrode. (c) Discharge/charge curves and (d) cycling performance of CNT/S-60% electrode.

This method is applicative for lower content KB/S-50% material and 1D material CNT/S-60%. All the electrodes show typical two discharge plateaus and one charge plateau (Fig. S5), which are consistent with the CV results. The discharge voltage plateaus slightly decline due to the increased overpotential at a higher discharge rate. Both electrodes show high areal specific capacity over 8 mAh/cm^2 after 30 cycles with high Coulombic efficiency.

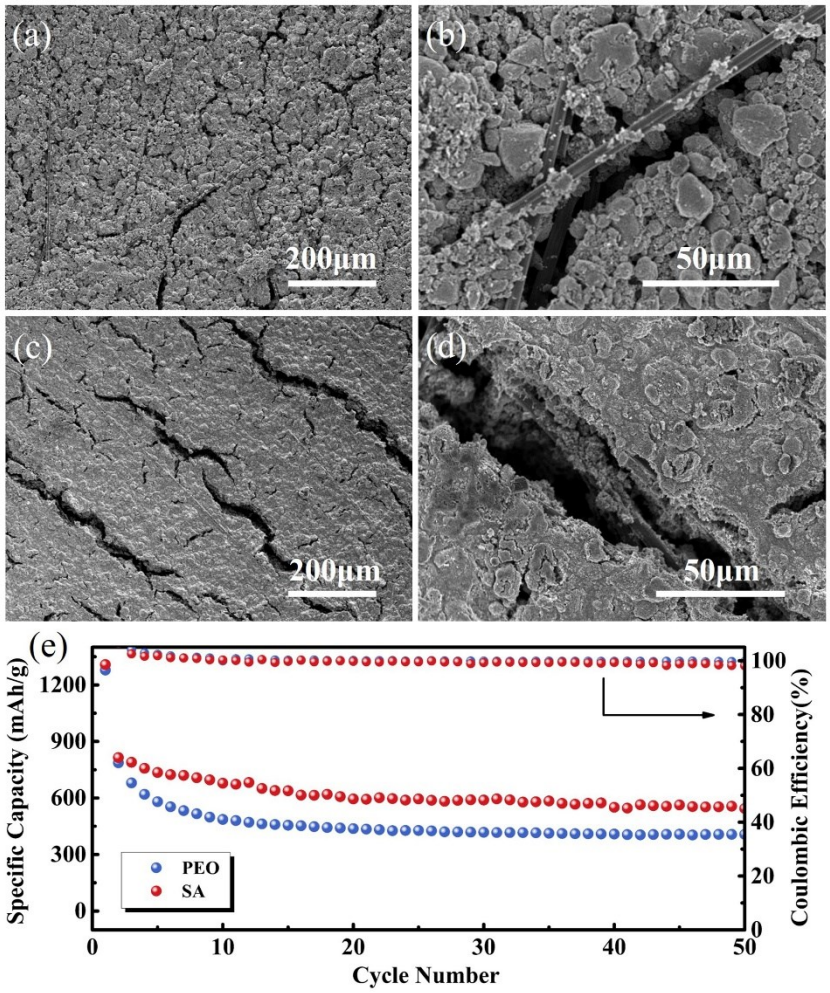

Fig. S13 Surface morphology of the sulfur cathode with different binder (a-b) PEO and (c-d) SA at different magnifications; (e) the cycle performance of thick electrode with sulfur loading of 10 mg cm^{-2} at 0.1C.

In order to demonstrate the general application of this method, different binders were used to prepared high loading cathode. Water-based binders such as PEO and SA with good cohesiveness can act as function binder for the high loading electrode. With the two binders, high loading sulfur cathode of above 10 mg/cm^2 also can be achieved. It can be seen that less cracks are formed on the electrode surface with PEO and SA binder, and the carbon fibers can also be found in the electrode (Fig. S6). It is

demonstrated that several water-based binders can be used to prepare the CF-sewed thick electrode. The electrode with PEO binder shows lower specific capacity of 407 mAh/g after 50 cycles at 0.1 C than that with SA binder which remains specific capacity of 545 mAh/g after 50 cycles. The lower specific capacity may be caused by the hindered ion transport channels through the hairline cracks which is vital for the utilization of active materials.

Table 1 comparison of the electrochemical performance in previous work

Cathode material	Current collector	Loading (mg/cm^2)	Rate C	Cycle Number	Areal Specific Capacity (mAh/cm^2)	Reference
CP/PCH/S cathode	3D carbon papers	9.0	0.25	300	7.0	[1]
NG-NCNT@NCS@S	thin Ni foam	10.2	1	150	5.43	[2]
NCF-S	NCF	4.5	0.2	200	4	[3]
CFC-S	CFC	6.7	~0.03	50	7	[4]
S@PCNF	PCNF	11.4	0.2	100	7.4	[5]
S/super P	Ni Foam	11.9 19.8	0.08 0.025	60 5	8.7 18	[6]
S/PEI-GO	carbon paper	7.3	0.2	200	4.7	[7]
NG/S	CNT/NFC	8.1	0.5	500	3.7	[8]
LRC/S@EFG	LRC	10.8	0.067	50	8	[9]

g-C_3N_4/S	AvCarb P50 paper	10.2	~0.06	50	5	[10]
C/S/MWCNT	carbon-coated aluminum foil	4.38	0.2	100	2.8	[11]
MPNC-S70	aluminum foil	4.2	~0.1	100	3.3	[12]
KB/S	aluminum foil	7.0	0.05	50	5.4	[13]
S/C	aluminum foil	13	0.1	50	15	[14]
Li_2S_6	CNFs	18.1	0.2	75	12	[15]
Li_2S_6	N,S-codoped GS	8.5	0.5	200	5.7	[16]
Li_2S_6	CNT/ACNF@ MnO_2	7.2	0.5	100	3.6	[17]
Li_2S_6	Carbon Cotton	61.4	0.1	50	43	[18]
KB/S	carbon-coated aluminum foil	10	0.1	96	7	This Work

References

[1] X. Wang, T. Gao, F. Han, Z. Ma, Z. Zhang, J. Li, C. Wang, Stabilizing high sulfur loading Li-S batteries by chemisorption of polysulfide on three-dimensional current collector, Nano Energy 30 (2016) 700-708.

[2] J. Wang, S. Cheng, W. Li, L. Jia, Q. Xiao, Y. Hou, Z. Zheng, H. Li, S. Zhang, L. Zhou, M. Liu, H. Lin, Y. Zhang, Robust electrical “highway” network for high mass loading sulfur cathode, Nano Energy 40 (2017) 390-398.

[3] W. Zhou, B. Guo, H. Gao, J.B. Goodenough, Low-Cost Higher Loading of a Sulfur Cathode,

Advanced Energy Materials 6 (2016) 1502059.

[4] L. Miao, W. Wang, K. Yuan, Y. Yang, A. Wang, A lithium-sulfur cathode with high sulfur loading and high capacity per area: a binder-free carbon fiber cloth-sulfur material, Chemical communications 50 (2014) 13231-13234.

[5] L. Qie, A. Manthiram, A facile layer-by-layer approach for high-areal-capacity sulfur cathodes, Advanced materials 27 (2015) 1694-1700.

[6] J. Liu, D.G.D. Galpaya, L. Yan, M. Sun, Z. Lin, C. Yan, C. Liang, S. Zhang, Exploiting a robust biopolymer network binder for an ultrahigh-areal-capacity Li–S battery, Energy Environ. Sci. (2017).

[7] X. Huang, K. Zhang, B. Luo, H. Hu, D. Sun, S. Wang, Y. Hu, T. Lin, Z. Jia, L. Wang, Polyethylenimine Expanded Graphite Oxide Enables High Sulfur Loading and Long-Term Stability of Lithium-Sulfur Batteries, Small (2019) e1804578.

[8] M. Yu, J. Ma, M. Xie, H. Song, F. Tian, S. Xu, Y. Zhou, B. Li, D. Wu, H. Qiu, R. Wang, Freestanding and Sandwich-Structured Electrode Material with High Areal Mass Loading for Long-Life Lithium-Sulfur Batteries, Advanced Energy Materials (2017) 1602347.

[9] Z. Li, J.T. Zhang, Y.M. Chen, J. Li, X.W. Lou, Pie-like electrode design for high-energy density lithium-sulfur batteries, Nature communications 6 (2015) 8850.

[10] Q. Pang, X. Liang, C.Y. Kwok, J. Kulisch, L.F. Nazar, A Comprehensive Approach toward Stable Lithium–Sulfur Batteries with High Volumetric Energy Density, Advanced Energy Materials (2016) n/a-n/a.

[11] P. Bhattacharya, M.I. Nandasiri, D. Lv, A.M. Schwarz, J.T. Darsell, W.A. Henderson, D.A. Tomalia, J. Liu, J.-G. Zhang, J. Xiao, Polyamidoamine dendrimer-based binders for high-loading

lithium-sulfur battery cathodes, Nano Energy 19 (2016) 176-186.

[12] J. Song, T. Xu, M.L. Gordin, P. Zhu, D. Lv, Y.-B. Jiang, Y. Chen, Y. Duan, D. Wang, Nitrogen-Doped Mesoporous Carbon Promoted Chemical Adsorption of Sulfur and Fabrication of High-Areal- Capacity Sulfur Cathode with Exceptional Cycling Stability for Lithium- Sulfur Batteries, Advanced Functional Materials 24 (2014) 1243-1250.

[13] X. Yang, Y. Chen, M. Wang, H. Zhang, X. Li, H. Zhang, Phase inversion: a universal method to create high-performance porous electrodes for nanoparticle-based energy storage devices, Advanced Functional Materials (2016) 201604229.

[14] M. Shaibani, M.S. Mirshekarloo, R. Singh, C.D. Easton, M.C.D. Cooray, N. Eshraghi, T. Abendroth, S. Dorfler, H. Althues, S. Kaskel, A.F. Hollenkamp, M.R. Hill, M. Majumder, Expansion-tolerant architectures for stable cycling of ultrahigh-loading sulfur cathodes in lithium-sulfur batteries, Science advances 6 (2020) eaay2757.

[15] L. Qie, C. Zu, A. Manthiram, A High Energy Lithium-Sulfur Battery with Ultrahigh-Loading Lithium Polysulfide Cathode and its Failure Mechanism, Advanced Energy Materials 6 (2016).

[16] G. Zhou, E. Paek, G.S. Hwang, A. Manthiram, Long-life Li/polysulphide batteries with high sulphur loading enabled by lightweight three-dimensional nitrogen/sulphur-codoped graphene sponge, Nature communications 6 (2015) 7760.

[17] H. Xu, L. Qie, A. Manthiram, An integrally-designed, flexible polysulfide host for high-performance lithium-sulfur batteries with stabilized lithium-metal anode, Nano Energy 26 (2016) 224-232.

[18] S.H. Chung, C.H. Chang, A. Manthiram, A Carbon-Cotton Cathode with Ultrahigh-Loading Capability for Statically and Dynamically Stable Lithium-Sulfur Batteries, ACS Nano (2016).